Exciton-driven renormalization of quasiparticle band structure in monolayer MoS₂

Yi Lin [1,*] Yang-hao Chan,[1,†] Woojoo Lee [2] Li-Syuan Lu,[4,5] Zhenglu Li [1] Wen-Hao Chang,[4,5] Chih-Kang Shih,[2]
Robert A. Kaindl,[1,‡] Steven G. Louie [1,3] and Alessandra Lanzara[1,3,§]

[1]*Materials Sciences Division, Lawrence Berkeley National Laboratory, Berkeley, California 94720, USA*
[2]*Department of Physics, The University of Texas at Austin, Austin, Texas 78712, USA*
[3]*Department of Physics, University of California, Berkeley, California 94720, USA*
[4]*Department of Electrophysics, National Yang Ming Chiao Tung University, Hsinchu 30010, Taiwan*
[5]*Research Center for Applied Sciences, Academia Sinica, Nankang, Taipei 11529, Taiwan*

Optical excitation serves as a powerful approach to control the electronic structure of layered van der Waals materials via many-body screening effects, induced by photoexcited free carriers, or via light-driven coherence, such as optical Stark and Bloch-Siegert effects. Although theoretical work has also pointed to an exotic mechanism of renormalizing band structure via excitonic correlations in bound electron-hole pairs (excitons), experimental observation of such exciton-driven band renormalization and the full extent of their implications is still lacking, largely due to the limitations of optical probes and the impact of screening effects. Here, by using extreme-ultraviolet time-resolved angle-resolved photoemission spectroscopy together with excitonic many-body theoretical calculations, we directly unmask the band renormalization effects driven by excitonic correlations in a monolayer semiconductor. We revealed a surprising bandgap opening, increased by 40 meV, and a simultaneous enhancement of band effective mass. Our findings unmask the exciton-driven mechanism toward the band engineering in photoexcited semiconducting materials, opening a playground to manipulate the transient energy states in layered quantum materials via optical controls of excitonic many-body correlations.

Excitons, excited bound electron-hole (e-h) pairs, have been widely observed in layered two-dimensional (2D) materials and have attracted significant interest, given their critical roles in both fundamental science and applications. With engineered dimensionality, dielectric environment, and excitation density, excitons and their derivative many-body quasiparticles have played significant roles in the functionality of optoelectrical and energy-harvesting devices [1–3] and in the realization of exotic quantum phases involving Mott physics [4–7], charge density wave formations [8–10], and Bose-Einstein condensations [10–12]. However, due to the intricate many-body nature of excitons, it remains an open question whether excitonic correlation renormalizes the single-particle band structure of materials, as is the case for other many-body interactions, such as electron-phonon [13,14], electron-electron [15], and electron-plasmon [16] interactions, as well as whether this could provide an inspiring direction of engineering matters in correlated phases.

The theoretical framework for addressing excitonic correlations by using the T-matrix self-energy in screened-ladder approximation was proposed four decades ago [17] and has often been used in recent theoretical studies of photoexcited layered semiconductors [18–22], which suggest extraordinary renormalization of the quasiparticle bandgap and dispersions. However, this type of band renormalization has been experimentally obscured. To provide experimental evidence of the exciton-driven band renormalization, we need a probe that can directly map the band structure of the material in both energy and momentum while also being able to probe exciton formation and dynamics. So far, most of optical experimental tools used in studying excitons [23] do not directly access the electron self-energy of the material $\Sigma(\mathbf{k}, \omega)$ in momentum space and hence cannot be used to study, if any, such band renormalization effects. In contrast, angle-resolved photoemission spectroscopy (ARPES) has been an ideal tool to measure material band structures. Only recently, time-resolved ARPES (trARPES) experiments have revealed that specific signatures of such an exciton bound state may indeed be present in the single-particle spectral function as part of the spectra in photoemission of layered tungsten dichalcogenides [24–27], inspiring opportunities for studying the exciton-driven band structure renormalization and engineering in materials.

Among the various material candidates, monolayer (ML) transition metal dichalcogenides (TMDCs) have been demonstrated as versatile platforms for realizing diverse excitonic and many-body phenomena via optical excitation [28–30], chemical doping [31,32], and electrical gating [33,34], which constitute promising techniques for exploring the exciton-driven band normalization. In addition, the versatility to place them on different substrates (from insulating to conducting),

---

*yilin@lbl.gov

†Current address: Institute of Atomic and Molecular Sciences, Academia Sinica, Taipei 106, Taiwan.

‡Current address: Department of Physics and CXFEL Laboratory, Arizona State University, Tempe, Arizona 85287, USA.
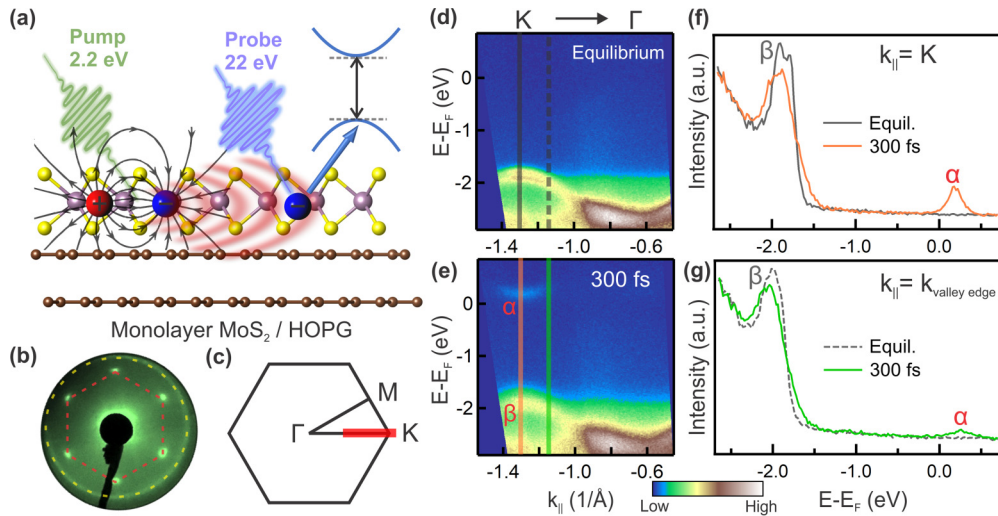
§ALanzara@lbl.gov

FIG. 1. (a) A schematic of high-harmonic-generation (HHG)-time-resolved angle-resolved photoemission spectroscopy (trARPES) experimental settings. (b) Low-energy electron diffraction (LEED) characterization of monolayer (ML) MoS_2/highly oriented pyrolytic graphite (HOPG) surface. Red (yellow) dashed lines denote the diffraction patterns from ML MoS_2 (HOPG). (c) Brillouin zone and high-symmetry points of ML MoS_2. Red solid line highlights the region where band structures are experimentally measured. Band structure measured for (d) equilibrium ($t = -500 \pm 100$ fs) and for (e) excited ($t = 300 \pm 100$ fs). Vertical lines in (d) and (e) denote the cuts at fixed momenta where energy distribution curves (EDCs) are extracted. (f) EDCs at the K point ($k = -1.29$ Å^{-1}) along the solid black line in (d) and the orange line in (e). (f) EDCs at $k = -1.14$ Å^{-1} along the dashed black line in (d) and the green line in (e). Greek letters in (e)–(g) highlight the major spectral features discussed in this paper.

together with the diverse choice of optical excitation density, provides the flexibility to operate in different regimes of interacting many-body e-h gas, which helps unmask the exciton-driven band renormalization from the strong screening effects of free carriers [35–46].

In this paper, we apply extreme-ultraviolet (XUV)-trARPES with high energy, momentum, and time resolution and in the low pump fluence regime to study the ultrafast electronic structure renormalization in ML MoS_2 on a substrate of conducting highly oriented pyrolytic graphite (HOPG) at 300 K. With a high-repetition-rate XUV-trARPES system [47,48], we discover exciton-driven ultrafast bandgap dynamics and band renormalization at the K valley of ML MoS_2. Combined with theoretical calculations, we provide evidence on the unique role that excitonic correlations play in inducing the exotic band renormalizations.

Figure 1(a) illustrates the schematic of our experiment. A highly oriented ML MoS_2/HOPG sample [see low-energy diffraction pattern in Fig. 1(b)] is excited by a visible 2.2 eV femtosecond pulse (pump, duration <130 fs) to create a transient excited state and then probed by a high-harmonic-generation (HHG)-derived pulse (probe) at 22.3 eV via ARPES as a function of time. Data were taken along the Γ-K direction [see Brillouin zone sketch in Fig. 1(c)]. More details on the experimental settings and sample preparation can be found in Secs. 1 and 2 in the Supplemental Material (SM) [49]. Figures 1(d) and 1(e) present the band structure for negative ($t = -500 \pm 100$ fs) and positive time delay ($t = 300 \pm 100$ fs). Throughout the paper, negative delay times corresponds to equilibrium before the pump pulse excites the sample. The most obvious change after the optical excitation is the appearance of the conduction band minima (CBM) at K. To highlight finer changes, in Figs. 1(f) and

1(g), we compare the equilibrium and excited state energy distribution curves (EDCs) at the center of the K valley $k = K$ (-1.29 Å^{-1}), corresponding to the momentum location of the valence band maximum (VBM) and CBM, and at a wave vector location away from K where the conduction band (CB) feature in the excited state is barely visible (which we call the edge of the K valley) $k = k_{\text{valley edge}}$ (-1.14 Å^{-1}). The equilibrium spectra at the K valley center [black curve in Fig. 1(f)] shows a splitting of the valence band (VB) peak ~ -1.8 eV (relative to the Fermi energy), denoted by the Greek letter β, due to the well-known spin-orbit coupling [46]. After the pump excitation, the CB gets populated, and a new peak (α), corresponding to the CBM, appears ~ 0.2 eV (orange curve). This is accompanied by a downshift of the VBM, followed by a depletion of its spectral weight, which makes it harder to resolve the spin-orbit splitting.

The ability to resolve both the CBM (α) and VBM (β) with significantly advanced data quality, compared with prior XUV-trARPES studies of layered MoS_2 [37,38,50–54], makes our experiment powerful to study the dynamics of the gap in response to excitation in a quantitative way. Figures 2(a) and 2(e) show the color maps of the spectral intensity as a function of delay time and binding energy at the K point and $k = k_{\text{valley edge}}$, taken along the vertical orange and green lines in Fig. 1(e), respectively. After the pump pulse ($t > 0$), a feature above the Fermi energy appears, which from our interpretation below corresponds to the CBM for $k = K$ spectra [in Fig. 2(a)] and the CB edge for the $k = k_{\text{valley edge}}$ spectra [in Fig. 2(e)]. This feature persists for picoseconds after the pump excitation. The excitation-induced energy position changes of both the CB and the VB can be extracted by fitting the EDC spectra with single or double peak functions (see methods of the fittings in the SM [49]) and are shown as
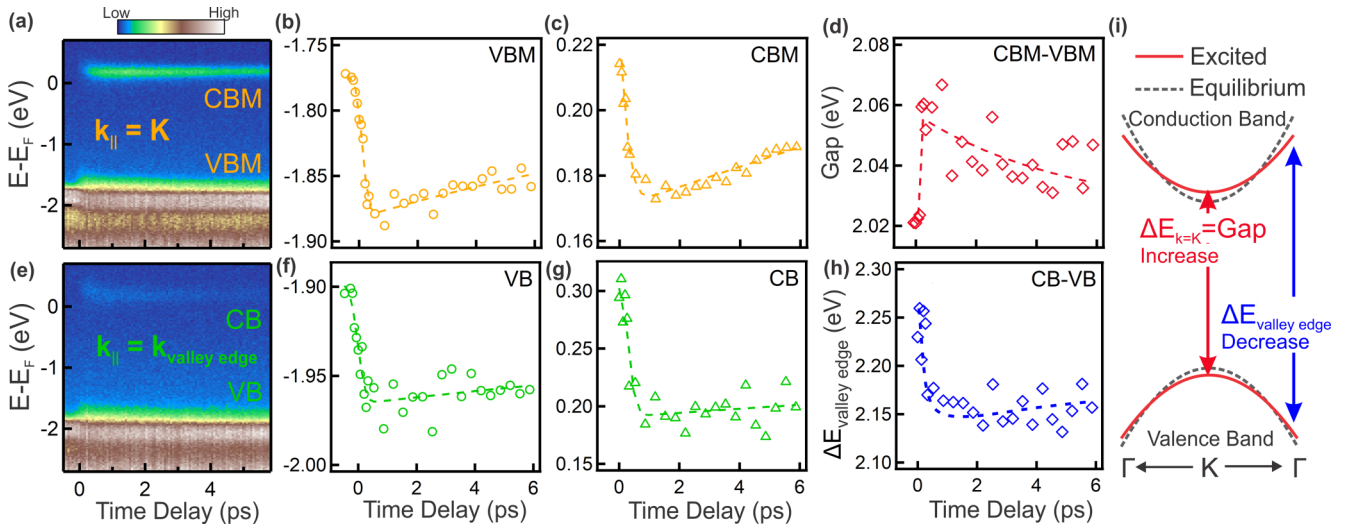
FIG. 2. Color map of the spectral intensity as a function of delay times and binding energy at (a) the K point ($k = -1.29 \pm 0.01$ Å^{-1}) and at (e) the K valley edge ($k = -1.14 \pm 0.01$ Å^{-1}). Energy-fitted band position in time for (b) the valence band maximum (VBM) and (c) the conduction band minimum (CBM) at the K point, and for (f) the top valence band (VB) and (g) the conduction band (CB) at $k = -1.14$ Å^{-1}. (d) Bandgap dynamics at K. (h) Band energy distance dynamics at the K valley edge ($k = -1.14$ Å^{-1}). Dashed lines in (b)–(h) are guides for the eye. (i) A schematic of nontrivial band structure renormalization manifesting the nonmonotonic **k**-dependent band energy distance dynamics in (d) and (h).

a function of delay time in Figs. 2(b) and 2(c) for $k = K$ and Figs. 2(f) and 2(g) for $k = k_{\text{valley edge}}$, respectively. Immediately after excitation, both higher branches of the spin-split VB and CB show a clear downshift in energy at the two momenta positions. The dynamics of the relative shift of the VB and CB at these two **k** points can be directly extracted from these data. At the K point, the relative difference is nothing else than the direct bandgap (ΔE_K = Gap), as shown in Fig. 2(d). Surprisingly, the data reveal an increase of the bandgap, up to 40 meV (from 2.02 to $\sim$2.06 eV) after the optical excitation, and then the increased gap starts to recover with a decay rate $\tau = 5.0 \pm 1.8$ ps. In contrast, at the edge of the discernable valley ($k = k_{\text{valley edge}}$), the energy separation between the CB and top VB ($\Delta E_{\text{valley edge}}$) decreases by $\sim$100 meV. The opposite direction between ΔE_K and $\Delta E_{\text{valley edge}}$ suggests that nonmonotonic **k**-dependent energy renormalization effects might be at play, as illustrated by the sketch in Fig. 2(i). It is important to note that our observed bandgap increase cannot be attributed to the known optical Stark or Bloch-Siegert effects [55,56], which lead to the increase of the optical gap (instead of the bandgap) due to the optically driven coherence, requiring the persistent presence of a light field (instead of excitonic many-body correlations).

To gain further insights on the **k**-dependent band renormalization, in Fig. 3, we provide a quantitative analysis of the dispersion and effective mass of the CB and VB after photoexcitation. Figures 3(a)–3(c) and 3(d)–3(f) show the color maps of the spectral intensity, as a function of energy and momentum, at different characteristic delay times, for the dispersion near the CBM and VBM, respectively. In Fig. 3(a), at $t = 0$ fs (defined by the center of the pump-probe cross-correlation), the pump excitation slightly populates the CB. At later delay time [Figs. 3(b) and 3(c)], the CB is gradually depopulated, after an initial increase of the photoemission intensity at the CBM due to the scattering of electrons from other k points.

Figures 3(g) and 3(h) report the dispersions of the CB and the upper branch of the split VB, respectively, obtained by fitting the EDC spectra. The data show a clear flattening of the dispersion at later delay time [compare the blue dashed curve (0 fs) with the red curve (1.5 ps)], leading to an increase of the CB effective mass by a factor of 3, from 0.71 m_e to 2.45 m_e (m_e = electron mass in vacuum), as shown in Fig. 3(i). This change occurs already within the first 1.5 ps after excitation, corresponding to the time window of the fast-declining edge in Fig. 2(c). We also note that such band flattening cannot be attributed to the temperature-dependent broadening of the Fermi-Dirac distribution (see details in Sec. 5.3 in the SM [49]). For the VB, a smaller scale of the flattening of the dispersion [Fig. 3(h), compare gray and red curves] and hence enhancement of the effective mass [Fig. 3(j)] is also observed. These apparently smaller enhancements might be affected by the decrease of the VB spectral weight in the transient state, making it hard to resolve the spin splitting of the two bands. The details and the physical causes of the asymmetrical behavior between the CB and VB are beyond the scope of this paper and require more future investigations.

The results shown so far point to the presence of strong photoexcitation-induced band renormalization, manifested by an increase of both the bandgap and effective mass. As discussed in detail below, we attribute these observations to the exciton-driven band renormalization, as schematically illustrated in Fig. 4(a). Clearly these exciton-driven effects are in striking contrast to the ones driven by the unbound photoexcited free carriers in Fig. 4(b), such as the large bandgap decrease that is attributed to the strong screening effects due to the high density of excited e-h gas as free carriers. Such a bandgap decrease has been explained by theoretical tools such as GW methods [57,58] and has been observed in (tr)ARPES studies of ML semiconductors by injecting high-density electron dopants [32] or high-fluence photoexcitation [37,50].
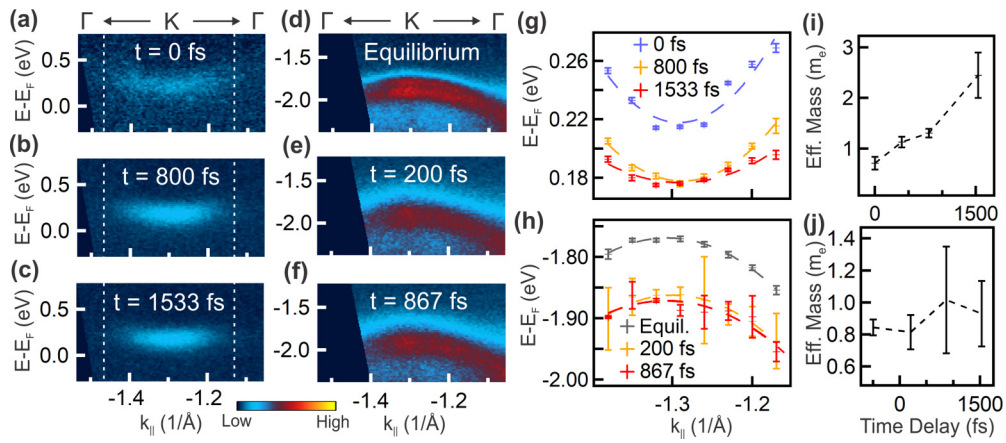
FIG. 3. Dispersion near the conduction band minimum (CBM) for (a) $t = 0$ fs, (b) $t = 800$ fs, and (c) $t = 1533$ fs. Dispersion of two bands near the valence band maximum (VBM) for (d) equilibrium ($t = -467$ fs), (e) $t = 200$ fs, and (f) $t = 867$ fs. (g) Parabolic curve fits for conduction band (CB) dispersions in (a)–(c). (h) Parabolic curve fits for upper valence band (VB) dispersions in (d)–(f). (i) Electron effective mass for the CB dispersions in time. (j) Hole effective mass for the upper VB dispersions in time.

However, it is critical to note that the free-carrier-driven mechanism alone does not fully account for our observations. Indeed, the unbound free carriers are expected to only drive a monotonic decrease of the bandgap for increasing carrier densities and therefore cannot explain our observation of the bandgap increase. Moreover, the excitation fluences in our experiment are in the range of a few tens of μJ/cm^2 (see the methods Sec. 2 in SM), which is $\sim$10–100 times lower than the fluences adopted in previous XUV-trARPES work on MoS$_2$ [37,38,50–54] (hundreds of μJ/cm^2 to mJ/cm^2). The resulting excitation densities in our experiment are expected to be beneath the Mott threshold which is believed to be mid to high 10^{12} cm^{-2} for ML MoS$_2$ [50].

To gain a full picture of what might drive the nontrivial renormalization effects reported here, it is necessary to consider the bound e-h pairs with excitonic correlations. To this end, we perform many-body theoretical calculations going beyond the free-carrier-driven picture. With the assumption that bound excitons with excitonic correlations are present in the excited e-h gas below the Mott threshold, we calculate the interacting single-particle spectral functions of ML MoS$_2$ at various excitation densities using a self-energy formalism, where the GW diagram and the T-matrix ladder diagrams are integrated to include the exciton-driven effects. The details of the self-energy construction are available in Secs. 3.2–3.4 in the SM [49]. We further employ the quasi-equilibrium
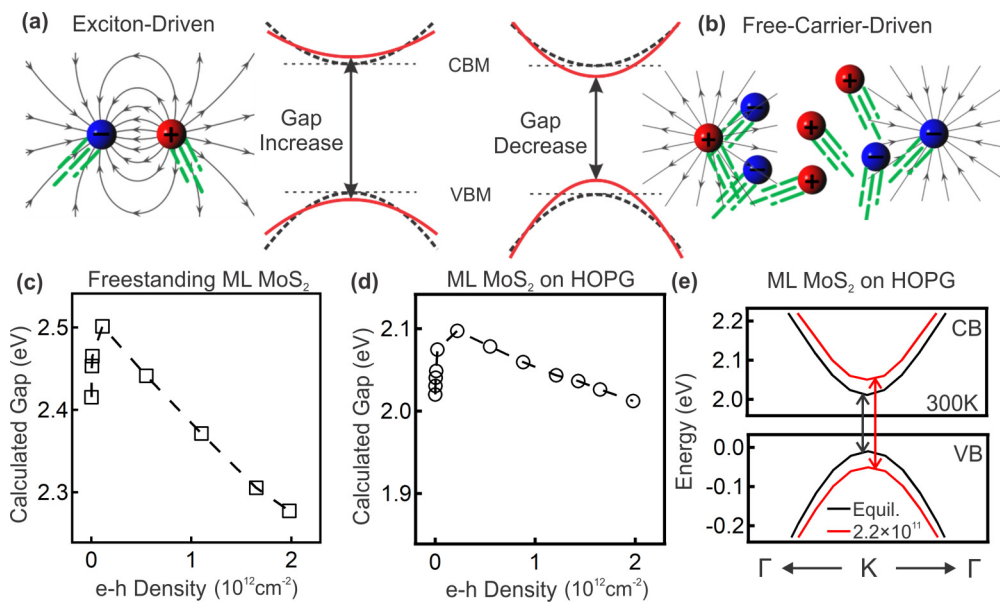

FIG. 4. A schematic of (a) exciton-driven bandgap increase and (b) free-carrier-driven bandgap decrease. Note that (a) and (b) are simplified to show the opposite trend of the gap and dispersion variations and do not imply a symmetrical behavior between the valence band (VB) and conduction band (CB) renormalization. Calculated gap as a function of electron-hole density for (c) freestanding monolayer (ML) MoS$_2$ and (d) ML MoS$_2$ on highly oriented pyrolytic graphite (HOPG). (e) Calculated CB and VB dispersions at two representative e-h density for ML MoS$_2$ on HOPG at 300 K. Black and red arrows denote the bandgap at equilibrium and the excited phases.

theory which assumes that the dynamics of the photoexcited electrons and holes change steadily after the optical excitation (see details in Sec. 3.1 in the SM [49]). Within this picture, we simulate the band renormalization as a function of densities of photoexcited electrons and holes.

In Fig. 4(c), we present the calculated quasiparticle bandgap of ML MoS_2 as a function of the excited e-h density. The inclusion of the excitonic correlations in the simulation leads to an appealing nonmonotonic behavior of the gap-density curve. When a small finite number of electrons and holes are excited and available to form excitons, we observe a sudden increase of the calculated bandgap up to several tens of millielectronvolts, followed by a decrease, as the carrier density further increases. The domelike increased-gap area at the low-density regime is the result of excitonic correlations and is responsible for the observation of the gap increase in Fig. 2(d).

To unmask experimentally the exciton-driven gap increase, we also need to consider the presence of the substrate effects. Environmental screening effects modify the effective dielectric constant in the sample via substrates or by encapsulating the 2D layer with other materials [59–61]. In the case of a conducting substrate, such as the HOPG utilized in this paper, the charge in the substrate screens the ML semiconductor and is known to drive a reduction of the quasiparticle bandgap up to ~200 meV from its freestanding value [59]. The bandgap reduction from that of a freestanding sample (theoretical bandgap ~2.4 eV) is indeed observed in our experiment, where the direct gap size with maximum populated CBM is 2.10 ± 0.02 eV at 80 K, in line with that in previous scanning tunneling spectroscopy (STS) work on a similar substrate at 77 K [62,63]. The fact that the gap size is comparable in both experiments, i.e., when measured without photoexcitation (as is the case in equilibrium STS experiments) or with photoexcitation (as in this trARPES study), confirms the role of the conducting substrate in modulating the response of the bandgap to photoexcitation.

To quantify the substrate effects and how this is reflected in our findings, in Fig. 4(d), we present the calculated quasiparticle bandgap of ML MoS_2 on a HOPG substrate as a function of the photoexcited e-h density. The gap-density curve presents a significantly gentler slope in the descending tail than that of the freestanding case in Fig. 4(c), which results in a broader dome of increased gap toward higher excitation density. The gentler slope could be understood in a way that the bandgap has been environmentally screened by the conducting substrate, so it becomes less subjective to the additional screening-induced gap decrease due to the photoexcited free carriers. Based on the calculated results, we conclude that the presence of the HOPG substrate helps extend the increased-gap dome over a broader range of excitation densities, providing a more ideal situation to experimentally search for the exciton-driven bandgap increase.

Another consequence of the excitonic correlations in theory is the band renormalization in the proximity of the CBM and VBM, as shown in Fig. 4(e) for two representative excitation densities. In addition to the increase of the bandgap discussed above, the calculations reveal a flattening of the VB

and CB after exciton formation (red curve) with respect to the equilibrium dispersion (black curves). This trend qualitatively agrees with our experimental observation of increased effective mass, discussed in Fig. 3.

In conclusion, we have provided experimental and theoretical evidence of exciton-driven renormalization effects in the electronic band structure of a ML semiconductor, leading to a transient enhancement of the bandgap and effective mass. The combination of the appropriate regime of excitation strength, the usage of the conducting substrate, and the supreme data quality have enabled us to unmask the exciton-driven band renormalization effects previously obscured. The excitonic mechanism can be applied to understand the emerging nonmonotonic bandgap behavior in a wide range of layered and bulk excitonic semiconducting and insulating materials [63–65] and opens up directions and pathways for optically driven ultrafast band engineering.

A.L. and Y.L. initiated and directed this research project. Y.L. and W.L. carried out the tr-ARPES and low-energy electron diffraction measurements. Y.-H.C. performed theoretical calculations, with supervision from S.G.L.; Y.-H.C., Z.L., and S.G.L. analyzed the theoretical results. The sample was prepared by L.-S.L. and W.L. for measurement, with supervision from C.-K.S. and W.-H.C.; Y.L. built the Optical Parametric Amplifier (OPA) dedicated to this paper and upgraded the pump-probe scheme from an XUV-trARPES setup developed by R.A.K. Data analyses were performed by Y.L. with help from A.L. The paper was written by Y.L. and A.L. with critical input from all other authors.

[1] A. Allain, J. Kang, K. Banerjee, and A. Kis, Electrical contacts to two-dimensional semiconductors, Nat. Mater. **14**, 1195 (2015).

[2] F. H. Koppens, T. Mueller, P. Avouris, A. C. Ferrari, M. S. Vitiello, and M. Polini, Photodetectors based on graphene, other two-dimensional materials and hybrid systems, Nat. Nanotechnol. **9**, 780 (2014).

[3] T. Mueller and E. Malic, Exciton physics and device application of two-dimensional transition metal dichalcogenide semiconductors, npj 2D Mater. Appl. **2**, 29 (2018).

[4] N. F. Mott, Metal-insulator transitions, Contemp. Phys. **14**, 401 (1973).

[5] T. Suzuki and R. Shimano, Exciton Mott Transition in Si Revealed by Terahertz Spectroscopy, Phys. Rev. Lett. **109**, 046402 (2012).

[6] L. Kappei, J. Szczytko, F. Morier-Genoud, and B. Deveaud, Direct Observation of the Mott Transition in an Optically Excited Semiconductor Quantum Well, Phys. Rev. Lett. **94**, 147403 (2005).

[7] M. Stern, V. Garmider, V. Umansky, and I. Bar-Joseph, Mott Transition of Excitons in Coupled Quantum Wells, Phys. Rev. Lett. **100**, 256402 (2008).

[8] K. Rossnagel, L. Kipp, and M. Skibowski, Charge-density-wave phase transition in $1T$-TiSe$_2$: Excitonic insulator versus band-type Jahn-Teller mechanism, Phys. Rev. B **65**, 235101 (2002).

[9] H. Cercellier, C. Monney, F. Clerc, C. Battaglia, L. Despont, M. G. Garnier, H. Beck, P. Aebi, L. Patthey, H. Berger *et al.*, Evidence for an Excitonic Insulator Phase in $1T$-TiSe$_2$, Phys. Rev. Lett. **99**, 146403 (2007).

[10] A. Kogar, M. S. Rak, S. Vig, A. A. Husain, F. Flicker, Y. I. Joe, L. Venema, G. J. MacDougall, T. C. Chiang, E. Fradkin *et al.*, Signatures of exciton condensation in a transition metal dichalcogenide, Science **358**, 1314 (2017).

[11] J. I. A. Li, T. Taniguchi, K. Watanabe, J. Hone, and C. R. Dean, Excitonic superfluid phase in double bilayer graphene, Nat. Phys. **13**, 751 (2017).

[12] Z. Wang, D. A. Rhodes, K. Watanabe, T. Taniguchi, J. C. Hone, J. Shan, and K. F. Mak, Evidence of high-temperature exciton condensation in two-dimensional atomic double layers, Nature (London) **574**, 76 (2019).

[13] A. Lanzara, P. V. Bogdanov, X. J. Zhou, S. A. Kellar, D. L. Feng, E. D. Lu, T. Yoshida, H. Eisaki, A. Fujimori, K. Kishio *et al.*, Evidence for ubiquitous strong electron-phonon coupling in high-temperature superconductors, Nature (London) **412**, 510 (2001).

[14] F. Giustino, M. L. Cohen, and S. G. Louie, Small phonon contribution to the photoemission kink in the copper oxide superconductors, Nature (London) **452**, 975 (2008).

[15] D. A. Siegel, C. H. Park, C. Hwang, J. Deslippe, A. V. Fedorov, S. G. Louie, and A. Lanzara, Many-body interactions in quasi-freestanding graphene, Proc. Natl. Acad. Sci. USA **108**, 11365 (2011).

[16] A. Bostwick, T. Ohta, T. Seyller, K. Horn, and E. Rotenberg, Quasiparticle dynamics in graphene, Nat. Phys. **3**, 36 (2006).

[17] H. Stolz and R. Zimmermann, Correlated pairs and a mass action law in two-component Fermi systems excitons in an electron-hole plasma, Phys. Status Solidi B **94**, 135 (1979).

[18] A. Steinhoff, M. Florian, M. Rosner, G. Schonhoff, T. O. Wehling, and F. Jahnke, Exciton fission in monolayer transition metal dichalcogenide semiconductors, Nat. Commun. **8**, 1166 (2017).

[19] E. Perfetto, D. Sangalli, A. Marini, and G. Stefanucci, First-principles approach to excitons in time-resolved and angle-resolved photoemission spectra, Phys. Rev. B **94**, 245303 (2016).

[20] A. Rustagi and A. F. Kemper, Photoemission signature of excitons, Phys. Rev. B **97**, 235310 (2018).

[21] D. Christiansen, M. Selig, E. Malic, R. Ernstorfer, and A. Knorr, Theory of exciton dynamics in time-resolved ARPES: Intra- and intervalley scattering in two-dimensional semiconductors, Phys. Rev. B **100**, 205401 (2019).

[22] N. H. Kwong, G. Rupper, and R. Binder, Self-consistent T-matrix theory of semiconductor light-absorption and luminescence, Phys. Rev. B **79**, 155205 (2009).

[23] G. Wang, A. Chernikov, M. M. Glazov, T. F. Heinz, X. Marie, T. Amand, and B. Urbaszek, Colloquium: Excitons in atomically thin transition metal dichalcogenides, Rev. Mod. Phys. **90**, 021001 (2018).

[24] J. Madéo, M. K. L. Man, C. Sahoo, M. Campbell, V. Pareek, E. L. Wong, A. Al-Mahboob, N. S. Chan, A. Karmakar, B. M. K. Mariserla *et al.*, Directly visualizing the momentum forbidden dark excitons and their dynamics in atomically thin semicondutors, Science **370**, 1199 (2020).

[25] R. Wallauer, R. Perea-Causin, L. Münster, S. Zajusch, S. Brem, J. Güdde, K. Tanimura, K.-Q. Lin, R. Huber, E. Malic *et al.*, Momentum-resolved observation of exciton formation dynamics in monolayer WS$_2$, Nano Lett. **21**, 5867 (2021).

[26] S. Dong, M. Puppin, T. Pincelli, S. Beaulieu, D. Christiansen, H. Hübener, C. W. Nicholson, R. P. Xian, M. Dendzik, Y. Deng *et al.*, Direct measurement of key exciton properties: Energy, dynamics, and spatial distribution of the wave function, Nat. Sci. **1**, e10010 (2021).

[27] M. K. L. Man, J. Madéo, C. Sahoo, K. Xie, M. Campbell, V. Pareek, A. Karmakar, E. L. Wong, A. Al-Mahboob, N. S. Chan *et al.*, Experimental measurement of the intrinsic excitonic wave function, Sci. Adv. **7**, eabg0192 (2021).

[28] D. Y. Qiu, F. H. da Jornada, and S. G. Louie, Optical Spectrum of MoS$_2$: Many-Body Effects and Diversity of Exciton States, Phys. Rev. Lett. **111**, 216805 (2013).

[29] A. Splendiani, L. Sun, Y. Zhang, T. Li, J. Kim, C. Y. Chim, G. Galli, and F. Wang, Emerging photoluminescence in monolayer MoS$_2$, Nano Lett. **10**, 1271 (2010).

[30] K. F. Mak, C. Lee, J. Hone, J. Shan, and T. F. Heinz, Atomically Thin MoS$_2$: A New Direct-Gap Semiconductor, Phys. Rev. Lett. **105**, 136805 (2010).

[31] S. Gao, Y. Liang, C. D. Spataru, and L. Yang, Dynamical excitonic effects in doped two-dimensional semiconductors, Nano Lett. **16**, 5568 (2016).

[32] J. Katoch, S. Ulstrup, R. J. Koch, S. Moser, K. M. McCreary, S. Singh, J. Xu, B. T. Jonker, R. K. Kawakami, A. Bostwick *et al.*, Giant spin-splitting and gap renormalization driven by trions in single-layer WS$_2$/h-BN heterostructures, Nat. Phys. **14**, 355 (2018).

[33] A. Chernikov, A. M. van der Zande, H. M. Hill, A. F. Rigosi, A. Velauthapillai, J. Hone, and T. F. Heinz, Electrical Tuning of Exciton Binding Energies in Monolayer WS$_2$, Phys. Rev. Lett. **115**, 126802 (2015).

[34] J. S. Ross, S. Wu, H. Yu, N. J. Ghimire, A. M. Jones, G. Aivazian, J. Yan, D. G. Mandrus, D. Xiao, W. Yao *et al.*,

Electrical control of neutral and charged excitons in a monolayer semiconductor, Nat. Commun. **4**, 1474 (2013).

[35] T. Eknapakul, P. D. King, M. Asakawa, P. Buaphet, R. H. He, S. K. Mo, H. Takagi, K. M. Shen, F. Baumberger, T. Sasagawa *et al.*, Electronic structure of a quasi-freestanding MoS_2 monolayer, Nano Lett. **14**, 1312 (2014).

[36] A. Chernikov, C. Ruppert, H. M. Hill, A. F. Rigosi, and T. F. Heinz, Population inversion and giant bandgap renormalization in atomically thin WS_2 layers, Nat. Photonics **9**, 466 (2015).

[37] S. Ulstrup, A. G. Cabo, J. A. Miwa, J. M. Riley, S. S. Gronborg, J. C. Johannsen, C. Cacho, O. Alexander, R. T. Chapman, E. Springate *et al.*, Ultrafast band structure control of a two-dimensional heterostructure, ACS Nano **10**, 6315 (2016).

[38] A. Grubisic Cabo, J. A. Miwa, S. S. Gronborg, J. M. Riley, J. C. Johannsen, C. Cacho, O. Alexander, R. T. Chapman, E. Springate, M. Grioni *et al.*, Observation of ultrafast free carrier dynamics in single layer MoS_2, Nano Lett. **15**, 5883 (2015).

[39] A. Steinhoff, M. Rosner, F. Jahnke, T. O. Wehling, and C. Gies, Influence of excited carriers on the optical and electronic properties of MoS_2, Nano Lett. **14**, 3743 (2014).

[40] Y. Park, S. W. Han, C. C. S. Chan, B. P. L. Reid, R. A. Taylor, N. Kim, Y. Jo, H. Im, and K. S. Kim, Interplay between many body effects and Coulomb screening in the optical bandgap of atomically thin MoS_2, Nanoscale **9**, 10647 (2017).

[41] K. Asano and T. Yoshioka, Exciton–Mott physics in two-dimensional electron-hole systems: Phase diagram and single-particle spectra, J. Phys. Soc. Jpn. **83**, 084702 (2014).

[42] Y. Liang and L. Yang, Carrier Plasmon Induced Nonlinear Band Gap Renormalization in Two-Dimensional Semiconductors, Phys. Rev. Lett. **114**, 063001 (2015).

[43] L. Meckbach, T. Stroucken, and S. W. Koch, Giant excitation induced bandgap renormalization in TMDC monolayers, Appl. Phys. Lett. **112**, 061104 (2018).

[44] P. D. Cunningham, A. T. Hanbicki, K. M. McCreary, and B. T. Jonker, Photoinduced bandgap renormalization and exciton binding energy reduction in WS_2, ACS Nano **11**, 12601 (2017).

[45] E. A. Pogna, M. Marsili, D. De Fazio, S. Dal Conte, C. Manzoni, D. Sangalli, D. Yoon, A. Lombardo, A. C. Ferrari, A. Marini *et al.*, Photo-induced bandgap renormalization governs the ultrafast response of single-layer MoS_2, ACS Nano **10**, 1182 (2016).

[46] M. M. Ugeda, A. J. Bradley, S. F. Shi, F. H. da Jornada, Y. Zhang, D. Y. Qiu, W. Ruan, S. K. Mo, Z. Hussain, Z. X. Shen *et al.*, Giant bandgap renormalization and excitonic effects in a monolayer transition metal dichalcogenide semiconductor, Nat. Mater. **13**, 1091 (2014).

[47] J. H. Buss, H. Wang, Y. Xu, J. Maklar, F. Joucken, L. Zeng, S. Stoll, C. Jozwiak, J. Pepper, Y. D. Chuang *et al.*, A setup for extreme-ultraviolet ultrafast angle-resolved photoelectron spectroscopy at 50-kHz repetition rate, Rev. Sci. Instrum. **90**, 023105 (2019).

[48] H. Wang, Y. Xu, S. Ulonska, J. S. Robinson, P. Ranitovic, and R. A. Kaindl, Bright high-repetition-rate source of narrowband extreme-ultraviolet harmonics beyond 22 eV, Nat. Commun. **6**, 7459 (2015).

[49] See Supplemental Material at http://link.aps.org/supplemental/10.1103/PhysRevB.106.L081117 for details of sample growth, experimental settings, and computational methods, including Refs. [19,66–73].

[50] F. Liu, M. E. Ziffer, K. R. Hansen, J. Wang, and X. Zhu, Direct Determination of Band-Gap Renormalization in the Photoexcited Monolayer MoS_2, Phys. Rev. Lett. **122**, 246803 (2019).

[51] R. Wallauer, J. Reimann, N. Armbrust, J. Güdde, and U. Höfer, Intervalley scattering in MoS_2 imaged by two-photon photoemission with a high-harmonic probe, Appl. Phys. Lett. **109**, 162102 (2016).

[52] P. Hein, A. Stange, K. Hanff, L. X. Yang, G. Rohde, K. Rossnagel, and M. Bauer, Momentum-resolved hot electron dynamics at the $2H$-MoS_2 surface, Phys. Rev. B **94**, 205406 (2016).

[53] K. Volckaert, H. Rostami, D. Biswas, I. Marković, F. Andreatta, C. E. Sanders, P. Majchrzak, C. Cacho, R. T. Chapman, A. Wyatt *et al.*, Momentum-resolved linear dichroism in bilayer MoS_2, Phys. Rev. B **100**, 241406(R) (2019).

[54] F. Liu, Q. Li, and X. Y. Zhu, Direct determination of momentum-resolved electron transfer in the photoexcited van der Waals heterobilayer WS_2/MoS_2, Phys. Rev. B **101**, 201405(R) (2020).

[55] E. J. Sie, J. W. McIver, Y.-H. Lee, L. Fu, J. Kong, and N. Gedik, Valley-selective optical Stark effect in monolayer WS_2, Nat. Mater. **14**, 290 (2015).

[56] E. J. Sie, C. H. Lui, Y.-H. Lee, L. Fu, J. Kong, and N. Gedik, Large, valley-exclusive Bloch-Siegert shift in monolayer WS_2, Science **355**, 1066 (2017).

[57] M. S. Hybertsen and S. G. Louie, Electron correlation in semiconductors and insulators: band gaps and quasiparticle energies, Phys. Rev. B **34**, 5390 (1986).

[58] J. Deslippe, G. Samsonidze, D. A. Strubbe, M. Jain, M. L. Cohen, and S. G. Louie, BERKELEYGW: A massively parallel computer package for the calculation of the quasiparticle and optical properties of materials and nanostructures, Comput. Phys. Commun. **183**, 1269 (2012).

[59] A. Raja, A. Chaves, J. Yu, G. Arefe, H. M. Hill, A. F. Rigosi, T. C. Berkelbach, P. Nagler, C. Schuller, T. Korn *et al.*, Coulomb engineering of the bandgap and excitons in two-dimensional materials, Nat. Commun. **8**, 15251 (2017).

[60] S. Park, N. Mutz, T. Schultz, S. Blumstengel, A. Han, A. Aljarb, L.-J. Li, E. J. W. List-Kratochvil, P. Amsalem, and N. Koch, Direct determination of monolayer MoS_2 and WSe_2 exciton binding energies on insulating and metallic substrates, 2D Materials **5**, 025003 (2018).

[61] A. Chaves, J. G. Azadani, H. Alsalman, D. R. da Costa, R. Frisenda, A. J. Chaves, S. H. Song, Y. D. Kim, D. He, J. Zhou *et al.*, Bandgap engineering of two-dimensional semiconductor materials, npj 2D Mater. Appl. **4**, 29 (2020).

[62] C. Zhang, A. Johnson, C. L. Hsu, L. J. Li, and C. K. Shih, Direct imaging of band profile in single layer MoS_2 on graphite: Quasiparticle energy gap, metallic edge states, and edge band bending, Nano Lett. **14**, 2443 (2014).

[63] W. Lee, Y. Lin, L. S. Lu, W. C. Chueh, M. Liu, X. Li, W. H. Chang, R. A. Kaindl, and C. K. Shih, Time-resolved ARPES determination of a quasi-particle band gap and hot electron dynamics in monolayer MoS_2, Nano Lett. **21**, 7363 (2021).

[64] M. Puppin, C. W. Nicholson, C. Monney, Y. Deng, R. P. Xian, J. Feldl, S. Dong, A. Dominguez, H. Hübener, A. Rubio *et al.*, Excited-state band structure mapping, Phys. Rev. B **105**, 075417 (2022).

[65] S. Mor, M. Herzog, D. Golez, P. Werner, M. Eckstein, N. Katayama, M. Nohara, H. Takagi, T. Mizokawa, C. Monney *et al.*, Ultrafast Electronic Band Gap Control in an Excitonic Insulator, Phys. Rev. Lett. **119**, 086401 (2017).

[66] E. Perfetto, D. Sangalli, A. Marini, and G. Stefanucci, Nonequilibrium Bethe-Salpeter equation for transient photoabsorption spectroscopy, Phys. Rev. B **92**, 205304 (2015).

[67] L. Perfetti, P. A. Loukakos, M. Lisowski, U. Bovensiepen, H. Eisaki, and M. Wolf, Ultrafast Electron Relaxation in Superconducting $Bi_2Sr_2CaCu_2O_{8+\delta}$ by Time-Resolved Photoelectron Spectroscopy, Phys. Rev. Lett. **99**, 197001 (2007).

[68] J. Tao, R. P. Prasankumar, E. E. M. Chia, A. J. Taylor, and J.-X. Zhu, Theory of ultrafast quasiparticle dynamics in high-temperature superconductors: the dependence on pump fluence, Phys. Rev. B **85**, 144302 (2012).

[69] Y. Wang and F.-C. Zhang, Momentum-resolved electronic relaxation dynamics in d-wave superconductors, Phys. Rev. B **89**, 094519 (2014).

[70] D. Sangalli, S. Dal Conte, C. Manzoni, G. Cerullo, and A. Marini, Nonequilibrium optical properties in semiconductors from first principles: a combined theoretical and experimental study of bulk silicon, Phys. Rev. B **93**, 195205 (2016).

[71] A. Molina-Sánchez, D. Sangalli, L. Wirtz, and A. Marini, *Ab initio* calculations of ultrashort carrier dynamics in two-dimensional materials: valley depolarization in single-layer WSe_2, Nano Lett. **17**, 4549 (2017).

[72] M. Rohlfing and S. G. Louie, Electron-hole excitations and optical spectra from first principles, Phys. Rev. B **62**, 4927 (2000).

[73] C. Friedrich, A. Schindlmayr, and S. Blügel, Efficient calculation of the Coulomb matrix and its expansion around within the FLAPW method, Comput. Phys. Commun. **180**, 347 (2009).